electronics

Article

Performance Evaluation of UAV-Based NOMA Networks with Hardware Impairment

Chung Ho Duc [1], Sang Quang Nguyen [2], Chi-Bao Le [3] and Ngo Tan Vu Khanh [4,*]

1 Institute of Engineering and Technology, Thu Dau Mot University, Thu Dau Mot 75109, Vietnam; hoducchung@tdmu.edu.vn
2 Department of Science and International Cooperation, Ho Chi Minh Minh City University of Transport, Ho Chi Minh City 72308, Vietnam; sang.nguyen@ut.edu.vn
3 Faculty of Electronics Technology, Industrial University of Ho Chi Minh City (IUH), Ho Chi Minh City 71408, Vietnam; lechibao@iuh.edu.vn
4 Department of Ecommerce Technology, School of Business Information Technology, University of Economics Ho Chi Minh City, Ho Chi Minh City 70000, Vietnam
* Correspondence: khanhntv@ueh.edu.vn

Abstract: In this paper, we evaluate the outage performance of a non-orthogonal multiple access (NOMA)-enabled unmanned aerial vehicle (UAV) where two users on the ground are simultaneously served by a UAV for a spectral efficiency purpose. In practice, hardware impairments at the transceiver cause distortion noise, which results in the performance loss of wireless systems. As a consequence, hardware impairment is an unavoidable factor in the system design process. Hence, we take into account the effects of hardware impairment (HI) on the performance of the proposed system. In this setting, to evaluate the system performance, the closed-form expressions of the outage probability of two NOMA users and the ergodic capacity are derived as well as their asymptotic expressions for a high signal-to-noise ratio (SNR). Finally, based on Monte-Carlo simulations, we verify the analytical expressions and investigate the effects on the main system parameters, i.e., the transmit SNR and level of HI, on the system performance metrics. The results show that the performance for the near NOMA user is better than of that for the far NOMA user in the case of perfect hardware; however, in the case of hardware impairment, an inversion happens at a high transmit power of the UAV in terms of the ergodic capacity.

Keywords: unmanned aerial vehicle (UAV); NOMA; hardware impairments; successive interference cancellation; outage probability; ergodic rate

Citation: Duc, C.H.; Nguyen, S.Q.; Le, C.-B.; Khanh, N.T.V. Performance Evaluation of UAV-Based NOMA Networks with Hardware Impairment. *Electronics* **2022**, *11*, 94. https://doi.org/10.3390/electronics11010094

Academic Editor: Alexey Vinel

Received: 20 October 2021
Accepted: 24 December 2021
Published: 28 December 2021

1. Introduction

In recent years, the use of UAVs in a wide range of civil and defense applications, such as search and rescue, cargo transport, and precision agriculture, has experienced unprecedented growth [1,2]. Further, two types of UAV, i.e., the rotary-wing type or fixed-wing type, are classified [3]. A UAV of the rotary-wing type equipped with multiple propellers can hover over fixed locations. A UAV of the fixed-wing type only flies in a path having a curvilinear form at a certain height, but cannot move along the vertical axis. Due to less power consumption of the fixed-wing type UAV compared with the rotary-wing type UAV, the fixed-wing type UAV is expected to be a potential solution for power-limited temporal wireless networks. Therefore, many deployment applications using UAVs in wireless communication networks have been studied, i.e., cooperative UAV networks [4], caching in wireless networks [5], and physical layer security [6].

Downlink non-orthogonal multiple access (NOMA) enables multiuser communication with the same frequency, which improves bandwidth utilization based on the design of the communication resources [7,8]. A few recent works have investigated the performance improvement of UAV-enabled communications systems based on the use of NOMA. In [9], the authors evaluated the outage probabilities of two ground NOMA users for a UAV base station communication system. The capacity region of a UAV support system with two ground users was studied; moreover, the trajectory and transmission power of the UAVs were jointly optimized [10]. The authors in [11] achieved the maximum sum-rate of a NOMA-based UAV by optimizing the power allocation and the UAV altitude. To improve the performance of a UAV-NOMA system, the authors in [12] designed a UAV deployment and power allocation scheme. A solution was proposed to maximize the number of users of a NOMA-enabled UAV while satisfying a quality service experience, by jointly optimizing the location design, admission control and power allocation [13]. An algorithm for minimizing the UAV mission completion time based on jointly optimizing the UAV trajectory and UAV ground base stations was designed in [14]. The energy efficiency of a mmWave-enabled NOMA-UAV system was maximized by optimizing the UAV position, hybrid precoding and power allocation in [15]. The UAV trajectory and the NOMA precoding were optimized to maximize the sum rate of a multiple user NOMA system in [16].

However, these works bypassed the problem of hardware impairment (HI) at the transmitters and receivers, while in practice the HI issue has a significant effect on system performance. HIs due to the phase noise of radio frequency components have been extensively investigated and modeled as additive distortion noise [17] and/or as a nonlinear polynomial multiplicative factor [18]. Considering HIs, a cognitive satellite–terrestrial network with multiple primary users was analyzed for outage performance in [19]. In [20], the outage probability and ergodic capacity under the effect of HIs on cooperative NOMA networks were derived. Over Rician fading channels, the effects of HIs on the NOMA cooperative duplex (FD) was examined [21]. However, the contents of these works did not mention UAVs in their systems, which was the motivation for us to study the influence of HIs on a UAV-based system.

In this paper, for more practical deployment, we consider a UAV system with regard to the HI issue where two ground users communicate with the UAV via a NOMA technique to improve the spectral usage.

The key contributions of this paper are listed as follows:

- Unlike in [9–14,17–21], where HIs were ignored and UAVs were absent, respectively, we investigate the outage performance, i.e., outage probability and ergodic capacity, of a UAV-based system consisting of two NOMA users and based on formulating mathematical equations with coefficients representing HI. Moreover, this is the first time a UAV-based system with HI issues has been considered.
- The performance of the proposed system is evaluated based on derivations of the closed-form expressions of the outage probability and ergodic capacity. To verify the derived expressions, we use Monte-Carlo simulations.
- The effects of HI on the proposed system are carefully investigated to provide a guideline for UAV-based system design. The results show that under the effects of HI, in terms of the ergodic capacity, the performance of the far user is better than that of the near user at a high transmit power of the UAV.

In Section 2, we describe the system model. The performance analysis is presented in Section 3. Section 4 investigates the ergodic capacity of the system. Section 4 shows numerical results. Finally, a conclusion for the obtained results is presented in Section 5.

2. System Model

We consider an UAV-enabled system where the UAV communicates with two NOMA users, i.e., U_1, U_2, as shown in Figure 1.

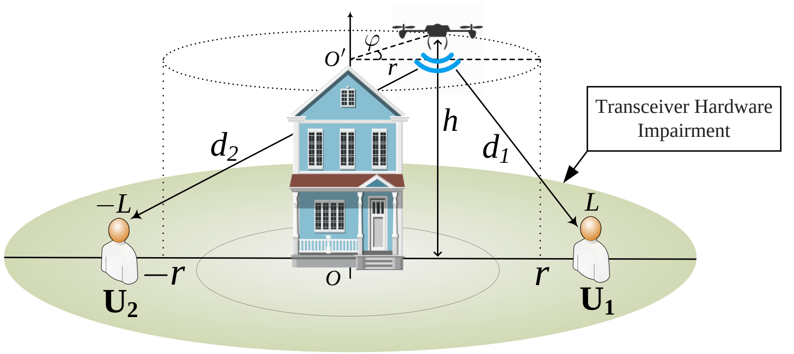

Figure 1. System model of UAV-enabled systems.

Such a UAV maintains a constant velocity v, a circular trajectory of radius r, and an altitude h while flying. The angle of the UAV position in the UAV circle is denoted by φ, then the location of the UAV is represented as UAV$(rcos\varphi, rsin\varphi, h)$. As a result, the Euclidean distance between users U_1 and U_2 and the UAV may be calculated as follows [9]

$$\bar{d}_1 = \sqrt{h^2 + r^2 + L^2 - 2rL\cos\varphi}, \tag{1a}$$

$$\bar{d}_2 = \sqrt{h^2 + r^2 + L^2 + 2rL\cos\varphi}. \tag{1b}$$

Finally, $\mathbb{P}_{LoS}(\theta_k)$ and $P_{NLoS}(\theta_k) = 1 - P_{LoS}(\theta_k)$ represent the line-of-sight (LoS) and the non-line-of-sight (NLoS) probability, respectively. These last two quantities are obtained from the following formula (Equation (3) in [22]).

$$\mathbb{P}_{LoS}(\theta_k) = \frac{1}{1+pe^{-q(\theta_k - p)}} \quad ,k \in \{1,2\} \tag{2}$$

where p and q are constant values depending on the environment and $\theta_k = \arcsin\left(\frac{H}{d_k}\right)$ is the so-called elevation angle of the UAV with respect to each user (Equation (2) in [11]).

The corresponding observation at U_i can be expressed as in [23]

$$\bar{y}_{U_i} = \frac{\bar{h}_i}{\sqrt{\bar{d}_i^{\alpha}}}\left(\sqrt{P\varpi_1}\bar{x}_1 + \sqrt{P\varpi_2}\bar{x}_2 + \bar{\eta}_{U_i}\right) + \bar{n}_{U_i} \quad ,i \in \{1,2\}, \tag{3}$$

where $\bar{h}_i \sim \mathcal{CN}(\mu_i, 2\sigma^2)$, α is the path loss exponent, η_{U_i} is the distortion noise caused by the UAV which is shown as $\bar{\eta}_{U_i} \sim \mathcal{CN}\left(0, \kappa_{U_1}^2\varpi_1 P + \kappa_{U_2}^2\varpi_2 P\right)$ in [24], and $\bar{n}_{U_i} \sim \mathcal{CN}(0, N_0)$ is the additive complex white Gaussian noise (AWGN).

With the help of (3), the signal-to-interference plus noise-and-distortion ratio (SINDR) at U_1 for signal $\bar{x}_2$ can be written as

$$\begin{aligned} \bar{\gamma}_{U_1,\bar{x}_2} =& \frac{\varpi_2 P\bar{d}_1^{-\alpha}\gamma_1}{N_0 + P\bar{d}_1^{-\alpha}\gamma_1\left[\kappa_{U_2}^2\varpi_2 + \left(1+\kappa_{U_1}^2\right)\varpi_1\right]} \\ =& \frac{\varpi_2\rho\bar{d}_1^{-\alpha}\gamma_1}{1 + \rho\bar{d}_1^{-\alpha}\gamma_1\left[\kappa_{U_2}^2\varpi_2 + \left(1+\kappa_{U_1}^2\right)\varpi_1\right]}, \end{aligned} \tag{4}$$

where $\gamma_1 \triangleq |\bar{h}_1|^2$ and $\rho = P/N_0$ are the transmit SNRs at the NOMA users.

The signal-to-noise and distortion ratio (SNDR) of decoding $\bar{x}_1$ at U_1 can be given as

$$\bar{\gamma}_{U_1,\bar{x}_1} = \frac{\varpi_1\rho\bar{d}_1^{-\alpha}\gamma_1}{1 + \rho\bar{d}_1^{-\alpha}\gamma_1\left[\kappa_{U_2}^2\varpi_2 + \kappa_{U_1}^2\varpi_1\right]}. \tag{5}$$

Next, U_2 can detect $\bar{x}_2$ by treating $\bar{x}_1$ as a noise, and the received SINR at U_2 is given by

$$\bar{\gamma}_{U_2,\bar{x}_2} = \frac{\varpi_2 \rho \bar{d}_2^{-\alpha} \gamma_2}{1 + \rho \bar{d}_2^{-\alpha} \gamma_2 \left[\kappa_{U_2}^2 \varpi_2 + \left(1 + \kappa_{U_1}^2\right) \varpi_1 \right]}, \tag{6}$$

where $\gamma_2 \triangleq |\bar{h}_2|^2$.

3. Performance Analysis

In this section, we first introduce the channel model, then evaluate the performance of the proposed system based on two metrics, i.e., the outage probabilities of the users and the throughput system.

3.1. The Channel Model

In this subsection, the wireless channels between UAVs and ground users are expected to endure small-scale fading and large-scale route loss as in this work [25]. The presence of a robust line-of-sight (LoS) route characterizes a UAV-to-ground link channel in general. As a result, the Rician distribution is applied to a UAV-to-ground link channel with LoS and multipath scatterers at the ground receiver. As a result, a non-central chi-square distribution with two degrees of freedom is used to represent the probability distribution function (pdf) of the unordered squared channel gain $\gamma_i, i \in \{1,2\}$ [26].

$$f_{|\gamma_i|^2}(x) = \phi_i e^{-K_i} e^{-\phi_i x} I_0\left(2\sqrt{K_i \phi_i x}\right), \tag{7}$$

where $\phi_i = (1 + K_i)/\Omega_i$, $I_0(x)$, $K_i \triangleq |\mu_i|^2 \big/ 2\sigma^2$ and $\Omega_i = \mathbb{E}\left\{|\gamma_i|^2\right\} = 1$ are the first-order modified Bessel function in the zeroth-order, the Rician factor, and the normalized average fading power, respectively. Based on Equation (8.445) in [27], (7) can be rewritten by

$$f_{|\gamma_i|^2}(x) = e^{-K_i} e^{-\phi_i x} \sum_{q=0}^{\infty} \frac{K_i^q \phi_i^{k+1}}{q!\Gamma(q+1)} x^q, \tag{8}$$

in which $\Gamma(x)$ is the gamma function. The CDF (cumulative distribution function) is written as

$$F_{|\gamma_i|^2}(x) = 1 - Q\left(\sqrt{2K_i}, \sqrt{2\phi_i x}\right), \tag{9}$$

where $Q(a,b)$ is the Marcum Q-function of the first-order [26]. Using Equation (4.35) in [26], Equation (8.445) in [27] and after some manipulation, the CDF of the Rician channels can be rewritten as

$$F_{|\gamma_i|^2}(x) = 1 - e^{-K_1 - \phi_i x} \sum_{k=0}^{\infty} \sum_{q=0}^{\infty} \frac{K_i^{k+q} \phi_i^q x^q}{q!\Gamma(k+q+1)}. \tag{10}$$

3.2. Outage Probability Analysis

Under the impacts of LoS and NLoS propagation, the outage probability (OP) of U_1 is determined as

$$\begin{aligned} \bar{\mathcal{P}}_{U_1} &= \mathbb{P}\left(\bar{\gamma}_{U_1,\bar{x}_2} < \bar{\varepsilon}_2 \cup \bar{\gamma}_{U_1,\bar{x}_1} < \bar{\varepsilon}_1\right) \\ &= 1 - \mathbb{P}\left(\bar{\gamma}_{U_1,\bar{x}_2} \geq \bar{\varepsilon}_2, \bar{\gamma}_{U_1,\bar{x}_1} \geq \bar{\varepsilon}_1\right), \end{aligned} \tag{11}$$

where $\bar{\varepsilon}_2 = 2^{2R_2} - 1$, $\bar{\varepsilon}_1 = 2^{2R_1} - 1$.

Proposition 1. *The OP of U_1 is calculated as:*

$$\bar{\mathcal{P}}_{U_1} = 1 - \mathcal{A}_1 - \mathcal{A}_2, \tag{12}$$

on the condition of $\varpi_2 > \bar{\varepsilon}_2\left[\kappa_{U_2}^2\varpi_2 + \left(1+\kappa_{U_1}^2\right)\varpi_1\right]$ *and* $\varpi_1 > \bar{\varepsilon}_1\left[\kappa_{U_2}^2\varpi_2 + \kappa_{U_1}^2\varpi_1\right]$, *where* $\mathcal{A}_1$ *and* $\mathcal{A}_2$ *are*

$$\begin{aligned}\mathcal{A}_1 &\stackrel{a}{=} \mathbb{P}_{LoS}(\theta_1)Q\left(\sqrt{2K_1}, \sqrt{2\phi_1\tilde{\chi}_{\max}}\right)\\ &\stackrel{b}{=} \mathbb{P}_{LoS}(\theta_1)e^{-K_1-\phi_1\tilde{\chi}_{\max}}\sum_{k=0}^{\infty}\sum_{q=0}^{\infty}\frac{K_1^{k+q}\phi_1^q\tilde{\chi}_{\max}^q}{q!\Gamma(k+q+1)},\end{aligned} \tag{13a}$$

$$\begin{aligned}\mathcal{A}_2 &\stackrel{a}{=} \mathbb{P}_{NLoS}(\theta_1)Q\left(\sqrt{2K_1}, \sqrt{2\phi_1\omega^{-1}\tilde{\chi}_{\max}}\right)\\ &\stackrel{b}{=} \mathbb{P}_{NLoS}(\theta_1)e^{-K_1-\phi_1\omega^{-1}\tilde{\chi}_{\max}}\sum_{k=0}^{\infty}\sum_{q=0}^{\infty}\frac{K_1^{k+q}\phi_1^q\tilde{\chi}_{\max}^q}{q!\omega\Gamma(k+q+1)}.\end{aligned} \tag{13b}$$

in which $\tilde{\chi}_2 = \frac{\bar{\varepsilon}_2}{\rho\bar{d}_1^{-\alpha}\left\{\varpi_2-\bar{\varepsilon}_2\left[\kappa_{U_2}^2\varpi_2+\left(1+\kappa_{U_1}^2\right)\varpi_1\right]\right\}}$, $\tilde{\chi}_1 = \frac{\bar{\varepsilon}_1}{\rho\bar{d}_1^{-\alpha}\left\{\varpi_1-\bar{\varepsilon}_1\left[\kappa_{U_2}^2\varpi_2+\kappa_{U_1}^2\varpi_1\right]\right\}}$, $\tilde{\chi}_{\max} = \max(\tilde{\chi}_2, \tilde{\chi}_1)$, $P_{LoS}(\theta_k)$ *and* $P_{NLoS}(\theta_k)$ *are given in* (2), *respectively.*

The OP of U_1 *is a function dependent on power coefficients, i.e.,* ϖ_1, ϖ_2, *the transmission rate of the two users, i.e.,* $\bar{\varepsilon}_1(R_1)$, $\bar{\varepsilon}_2(R_2)$, *the LoS and NLoS propagation conditions, i.e.,* $\mathbb{P}_{LoS}$ *and* $\mathbb{P}_{NLoS}$, *and the hardware impairment levels at the users, i.e.,* κ_{U_1} *and* κ_{U_2}.

Proof. From (11) we have the OP of U_1 which is calculated by

$$\begin{aligned}\bar{\mathcal{P}}_{U_1} =&\mathbb{P}\left(\bar{\gamma}_{U_1,x_2} < \bar{\varepsilon}_2 \cup \bar{\gamma}_{U_1,x_1} < \bar{\varepsilon}_1\right)\\ =&1-\mathbb{P}\left(\bar{\gamma}_{U_1,x_2} \geq \bar{\varepsilon}_2, \bar{\gamma}_{U_1,x_1} \geq \bar{\varepsilon}_1\right)\\ =&1-\mathbb{P}(\gamma_1 \geq \tilde{\chi}_{\max}),\end{aligned} \tag{14}$$

where $\tilde{\chi}_2 = \frac{\bar{\varepsilon}_2}{\rho\bar{d}_1^{-\alpha}\left\{\varpi_2-\bar{\varepsilon}_2\left[\kappa_{U_2}^2\varpi_2+\left(1+\kappa_{U_1}^2\right)\varpi_1\right]\right\}}$, $\tilde{\chi}_1 = \frac{\bar{\varepsilon}_1}{\rho\bar{d}_1^{-\alpha}\left\{\varpi_1-\bar{\varepsilon}_1\left[\kappa_{U_2}^2\varpi_2+\kappa_{U_1}^2\varpi_1\right]\right\}}$ and $\tilde{\chi}_{\max} = \max(\tilde{\chi}_2, \tilde{\chi}_1)$.

We may rewrite (14) as (15) based on the conditional probability.

$$\bar{\mathcal{P}}_{U_1} = 1 - \int_{\tilde{\chi}_{\max}}^{\infty} f_{\gamma_1}(x)dx. \tag{15}$$

Because each link's propagation is dependent on the LoS or NLoS propagation as in Equation (18) in [28], (15) is given by

$$\begin{aligned}\bar{\mathcal{P}}_{U_1} =&1-\left[\mathbb{P}_{LoS}(\theta_1)\int_{\tilde{\chi}_{\max}}^{\infty} f_{\gamma_1}(x)dx + \mathbb{P}_{NLoS}(\theta_1)\int_{\frac{\tilde{\chi}_{\max}}{\omega}}^{\infty} f_{\gamma_1}(x)dx\right]\\ =&1-\mathbb{P}_{LoS}(\theta_1)[1-F_{\gamma_1}(\tilde{\chi}_{\max})] - \mathbb{P}_{NLoS}(\theta_1)\left[1-F_{\gamma_1}\left(\frac{\tilde{\chi}_{\max}}{\omega}\right)\right],\end{aligned} \tag{16}$$

in which $\omega = 1$ for LoS propagation and $\omega < 1$ for NLoS propagation as in [29]. Then, plugging (9) and (10) into (16), $\mathcal{A}_1$ closed-form expression is obtained as (13a) and $\mathcal{A}_2$ as (13b).

The proof is completed. □

Next, from (6) the OP of U_2 is computed as follows:

$$\begin{aligned}\bar{\mathcal{P}}_{U_2} =&1-\mathbb{P}\left(\bar{\gamma}_{U_2,x_2} \geq \bar{\varepsilon}_2\right)\\ =&1-\mathbb{P}(\gamma_2 \geq \tilde{\chi}_2),\end{aligned} \tag{17}$$

where $\bar{\chi}_2 = \frac{\bar{\varepsilon}_2}{\rho \bar{d}_2^{-\alpha}\left\{\varpi_2 - \bar{\varepsilon}_2\left[\kappa_{U_2}^2\varpi_2 + \left(1+\kappa_{U_1}^2\right)\varpi_1\right]\right\}}$. Similarly, based on the solving of $\bar{\mathcal{P}}_{U_1}$, $\bar{\mathcal{P}}_{U_2}$ can be achieved as

$$\bar{\mathcal{P}}_{U_2} = 1 - \mathcal{A}_3 - \mathcal{A}_4, \tag{18}$$

in which

$$\begin{aligned}\mathcal{A}_3 &\overset{a}{=} \mathbb{P}_{LoS}(\theta_2) Q\left(\sqrt{2K_2}, \sqrt{2\phi_2\bar{\chi}_2}\right) \\ &\overset{b}{=} \mathbb{P}_{LoS}(\theta_2) e^{-K_2-\phi_2\bar{\chi}_2} \sum_{k=0}^{\infty}\sum_{q=0}^{\infty} \frac{K_2^{k+q}\phi_2^q\bar{\chi}_2^q}{q!\Gamma(k+q+1)},\end{aligned} \tag{19a}$$

$$\begin{aligned}\mathcal{A}_4 &\overset{a}{=} \mathbb{P}_{NLoS}(\theta_2) Q\left(\sqrt{2K_2}, \sqrt{2\phi_2\omega^{-1}\bar{\chi}_2}\right) \\ &\overset{b}{=} \mathbb{P}_{NLoS}(\theta_2) e^{-K_2-\phi_2\omega^{-1}\bar{\chi}_2} \sum_{k=0}^{\infty}\sum_{q=0}^{\infty} \frac{K_2^{k+q}\phi_2^q\bar{\chi}_2^q}{q!\omega\Gamma(k+q+1)}.\end{aligned} \tag{19b}$$

The OP of U_2 is a function dependent on power coefficients, i.e., ϖ_1, ϖ_2, its transmission rate, i.e., $\bar{\varepsilon}_2(R_2)$, the LoS and NLoS propagation conditions, i.e., $\mathbb{P}_{LoS}$ and $\mathbb{P}_{NLoS}$, and the hardware impairment levels at the users, i.e., κ_{U_1} and κ_{U_2}.

3.3. Asymptotic Analysis

Further, at high SNR $\rho \to \infty$, we may simplify the Marcum Q-function by applying the Taylor series expansion Equation (13) in [9]

$$Q\left(\sqrt{2K_i}, \sqrt{2\phi_i x}\right) \approx 1 - e^{-K_i}\phi_i x. \tag{20}$$

Invoking (20) into (18) and (17) and we get the following result

$$\bar{\mathcal{P}}_{U_1}^{\infty} = 1 - \mathbb{P}_{LoS}(\theta_1)\left(1 - e^{-K_1}\phi_1\bar{\chi}_{\max}\right) - \mathbb{P}_{NLoS}(\theta_2)\left(1 - e^{-K_1}\omega^{-1}\phi_1\bar{\chi}_{\max}\right), \tag{21}$$

and

$$\bar{\mathcal{P}}_{U_2}^{\infty} = 1 - \mathbb{P}_{LoS}(\theta_2)\left(1 - e^{-K_2}\phi_2\bar{\chi}_2\right) - \mathbb{P}_{NLoS}(\theta_2)\left(1 - e^{-K_2}\omega^{-1}\phi_2\bar{\chi}_2\right). \tag{22}$$

3.4. Throughput Analysis

Each user's throughput may be computed as follows

$$\bar{\tau}_{U_\star} = (1 - \bar{\mathcal{P}}_{U_\star})R_\star \quad , \star \in \{1,2\} \tag{23}$$

4. Ergodic Capacity

The ergodic total rate is a significant indicator for performance evaluation when user rates are calculated based on their channel circumstances.

The ergodic capacity of U_2 is computed as

$$\bar{\mathcal{C}}_2 = \mathbb{E}\{\log_2(1 + \bar{\gamma}_{U,\bar{x}_2})\}. \tag{24}$$

Proposition 2. *The closed-form equation for ergodic capacity at user U_2 is as follows*

$$\begin{aligned}\bar{\mathcal{C}}_2 =& \mathbb{P}_{LoS}(\theta_2)\sum_{k=0}^{\infty}\sum_{q=0}^{\infty}\frac{K_2^{k+q}\phi_2^q e^{-K_2}}{q!\Gamma(k+q+1)\ln 2}\left[\frac{1}{(\bar{\xi}+\bar{\zeta})^q} G_{1,2}^{2,1}\left(\frac{\phi_2}{\bar{\xi}+\bar{\zeta}}\middle| \begin{matrix}1-q-1\\ 1-q-1,0\end{matrix}\right)\right. \\ &\left.-\frac{1}{\bar{\zeta}^q}G_{1,2}^{2,1}\left(\frac{\phi_2}{\bar{\zeta}}\middle| \begin{matrix}1-q-1\\ 1-q-1,0\end{matrix}\right)\right] + \mathbb{P}_{NLoS}(\theta_2)\sum_{k=0}^{\infty}\sum_{q=0}^{\infty}\frac{K_2^{k+q}\phi_2^q e^{-K_2}}{q!\Gamma(k+q+1)\ln 2} \\ &\times\left[\frac{1}{\omega^q(\bar{\xi}+\bar{\zeta})^q}G_{1,2}^{2,1}\left(\frac{\phi_2}{\omega(\bar{\xi}+\bar{\zeta})}\middle| \begin{matrix}1-q-1\\ 1-q-1,0\end{matrix}\right) - \frac{1}{\omega^q\bar{\zeta}^q}G_{1,2}^{2,1}\left(\frac{\phi_2}{\omega\bar{\zeta}}\middle| \begin{matrix}1-q-1\\ 1-q-1,0\end{matrix}\right)\right],\end{aligned} \tag{25}$$

where $G_{p,q}^{m,n}[.]$ is the Meijer G-function in Equation (9.301) in [27], $\bar{\xi} = \rho \bar{d}_2^{-\alpha}\varpi_2$ and $\bar{\zeta} = \rho \bar{d}_2^{-\alpha}\left[\kappa_{U_2}^2\varpi_2 + \left(1+\kappa_{U_1}^2\right)\varpi_1\right]$. The ergodic capacity at U_2 is a function dependent on power coefficients, i.e., ϖ_1, ϖ_2, the LoS and NLoS propagation conditions, i.e., $\mathbb{P}_{LoS}$ and $\mathbb{P}_{NLoS}$, and the hardware impairment levels at the users, i.e., κ_{U_1} and κ_{U_2}, $\omega = 1$ represents LoS propagation and $\omega < 1$ represents NLoS propagation.

Proof. We have (26) if we put (6) into it.

$$\begin{aligned}\bar{\mathcal{C}}_2 =& \mathbb{E}\{\log_2(1+\bar{\gamma}_{U_2,\bar{x}_2})\} \\ =& \frac{1}{\ln 2}\int_0^\infty \frac{1}{1+x}\left[1 - F_{\bar{\gamma}_{U_2,\bar{x}_2}}(x)\right]dx \\ =& \frac{1}{\ln 2}\int_0^{\frac{\bar{\xi}}{\bar{\zeta}}} \frac{1}{1+x}\left[1 - F_{\gamma_2}\left(\frac{x}{\bar{\xi}-\bar{\zeta}x}\right)\right]dx,\end{aligned} \tag{26}$$

where $\bar{\xi} = \rho \bar{d}_2^{-\alpha}\varpi_2$ and $\bar{\zeta} = \rho \bar{d}_2^{-\alpha}\left[\kappa_{U_2}^2\varpi_2 + \left(1+\kappa_{U_1}^2\right)\varpi_1\right]$. It's worth noting that if $x > \frac{\bar{\xi}}{\bar{\zeta}}$, $\bar{\mathcal{C}}_2 = 0$.

In (26), by the variable changing $t \leftarrow \frac{x}{\bar{\xi}-\bar{\zeta}x}$ and after a few steps, $\bar{\mathcal{C}}_2$ can then be written as

$$\bar{\mathcal{C}}_2 = \frac{1}{\ln 2}\int_0^\infty \left(\frac{1}{t+\left(\bar{\xi}+\bar{\zeta}\right)^{-1}} - \frac{1}{t+\bar{\zeta}^{-1}}\right)[1 - F_{\gamma_2}(t)]dt. \tag{27}$$

In (18), we have $F_{\gamma_2}(t)$ which can be expressed as

$$\begin{aligned}F_{\gamma_2}(t) =& 1 - \mathbb{P}_{LoS}(\theta_2)\Pr(\gamma_2 > t) - \mathbb{P}_{NLoS}(\theta_2)\Pr\left(\gamma_2 > \frac{t}{\omega}\right) \\ =& 1 - \mathbb{P}_{LoS}(\theta_2)e^{-K_2-\phi_2 t}\sum_{k=0}^{\infty}\sum_{q=0}^{\infty}\frac{K_2^{k+q}\phi_2^q t^q}{q!\Gamma(k+q+1)} \\ &- \mathbb{P}_{NLoS}(\theta_2)e^{-K_2-\omega^{-1}\phi_2 t}\sum_{k=0}^{\infty}\sum_{q=0}^{\infty}\frac{K_2^{k+q}\phi_2^q t^q}{q!\omega^q\Gamma(k+q+1)}.\end{aligned} \tag{28}$$

Submitting (28) into (27), $\bar{\mathcal{C}}_2$ is given as

$$\begin{aligned}\bar{\mathcal{C}}_2 =& \mathbb{P}_{LoS}(\theta_2)\sum_{k=0}^{\infty}\sum_{q=0}^{\infty}\frac{K_2^{k+q}\phi_2^q e^{-K_2}}{q!\Gamma(k+q+1)\ln 2}\underbrace{\left[\int_0^\infty \frac{e^{-\phi_2 t}t^q}{t+\left(\bar{\xi}+\bar{\zeta}\right)^{-1}}dt - \int_0^\infty \frac{e^{-\phi_2 t}t^q}{t+\bar{\zeta}^{-1}}dt\right]}_{\mathcal{B}_1} \\ &+ \mathbb{P}_{NLoS}(\theta_2)\sum_{k=0}^{\infty}\sum_{q=0}^{\infty}\frac{K_2^{k+q}\phi_2^q e^{-K_2}}{q!\omega^q\Gamma(k+q+1)\ln 2}\underbrace{\left[\int_0^\infty \frac{e^{-\omega^{-1}\phi_2 t}t^q}{t+\left(\bar{\xi}+\bar{\zeta}\right)^{-1}}dt - \int_0^\infty \frac{e^{-\omega^{-1}\phi_2 t}t^q}{t+\bar{\zeta}^{-1}}dt\right]}_{\mathcal{B}_2}.\end{aligned} \tag{29}$$

Using the following methods, the exponential function is represented by Meijer's G-function Equation (8.4.3.1) in [30]

$$e^{-\phi_2 t} = G_{0,1}^{1,0}\left(\phi_2 x \middle| \begin{array}{c} - \\ 0 \end{array}\right), \tag{30a}$$

$$e^{-\frac{\phi_2}{\omega}t} = G_{0,1}^{1,0}\left(\frac{\phi_2}{\omega}x \middle| \begin{array}{c} - \\ 0 \end{array}\right). \tag{30b}$$

Submitting (30a) and (30b) into (29), $\mathcal{B}_1$ and $\mathcal{B}_2$ are given as

$$\mathcal{B}_1 = \left[\int_0^\infty \frac{t^q}{t+(\bar{\xi}+\bar{\zeta})^{-1}} G_{0,1}^{1,0}\left(\phi_2 t \middle| \begin{matrix} - \\ 0 \end{matrix}\right)dt - \int_0^\infty \frac{t^q}{t+\bar{\zeta}^{-1}} G_{0,1}^{1,0}\left(\phi_2 t \middle| \begin{matrix} - \\ 0 \end{matrix}\right)dt\right], \tag{31a}$$

$$\mathcal{B}_2 = \left[\int_0^\infty \frac{t^q}{t+(\bar{\xi}+\bar{\zeta})^{-1}} G_{0,1}^{1,0}\left(\frac{\phi_2}{\omega} x \middle| \begin{matrix} - \\ 0 \end{matrix}\right)dt - \int_0^\infty \frac{t^q}{t+\bar{\zeta}^{-1}} G_{0,1}^{1,0}\left(\frac{\phi_2}{\omega} x \middle| \begin{matrix} - \\ 0 \end{matrix}\right)dt\right]. \tag{31b}$$

In the next step, with the help of the Equation (7.811.5) in [27], $\mathcal{B}_1$ and $\mathcal{B}_2$ are given by

$$\mathcal{B}_1 = \left[\frac{1}{(\bar{\xi}+\bar{\zeta})^q} G_{1,2}^{2,1}\left(\frac{\phi_2}{\bar{\xi}+\bar{\zeta}} \middle| \begin{matrix} 1-q-1 \\ 1-q-1,0 \end{matrix}\right) - \frac{1}{\bar{\zeta}^q} G_{1,2}^{2,1}\left(\frac{\phi_2}{\bar{\zeta}} \middle| \begin{matrix} 1-q-1 \\ 1-q-1,0 \end{matrix}\right)\right], \tag{32a}$$

$$\mathcal{B}_2 = \left[\frac{1}{(\bar{\xi}+\bar{\zeta})^q} G_{1,2}^{2,1}\left(\frac{\phi_2}{\omega(\bar{\xi}+\bar{\zeta})} \middle| \begin{matrix} 1-q-1 \\ 1-q-1,0 \end{matrix}\right) - \frac{1}{\bar{\zeta}^q} G_{1,2}^{2,1}\left(\frac{\phi_2}{\omega\bar{\zeta}} \middle| \begin{matrix} 1-q-1 \\ 1-q-1,0 \end{matrix}\right)\right]. \tag{32b}$$

Substituting the results of (32a) and (32b) into (29), we have the close-form ergodic capacity expression of U_2, given as

$$\begin{aligned}
\bar{C}_2 =& \mathbb{P}_{LoS}(\theta_2) \sum_{k=0}^{\infty}\sum_{q=0}^{\infty} \frac{K_2^{k+q}\phi_2^q e^{-K_2}}{q!\Gamma(k+q+1)\ln 2}\left[\frac{1}{(\bar{\xi}+\bar{\zeta})^q} G_{1,2}^{2,1}\left(\frac{\phi_2}{\bar{\xi}+\bar{\zeta}} \middle| \begin{matrix} 1-q-1 \\ 1-q-1,0 \end{matrix}\right)\right. \\
&\left. - \frac{1}{\bar{\zeta}^q} G_{1,2}^{2,1}\left(\frac{\phi_2}{\bar{\zeta}} \middle| \begin{matrix} 1-q-1 \\ 1-q-1,0 \end{matrix}\right)\right] + \mathbb{P}_{NLoS}(\theta_2) \sum_{k=0}^{\infty}\sum_{q=0}^{\infty} \frac{K_2^{k+q}\phi_2^q e^{-K_2}}{q!\Gamma(k+q+1)\ln 2} \\
&\times \left[\frac{1}{\omega^q(\bar{\xi}+\bar{\zeta})^q} G_{1,2}^{2,1}\left(\frac{\phi_2}{\omega(\bar{\xi}+\bar{\zeta})} \middle| \begin{matrix} 1-q-1 \\ 1-q-1,0 \end{matrix}\right) - \frac{1}{\omega^q\bar{\zeta}^q} G_{1,2}^{2,1}\left(\frac{\phi_2}{\omega\bar{\zeta}} \middle| \begin{matrix} 1-q-1 \\ 1-q-1,0 \end{matrix}\right)\right].
\end{aligned} \tag{33}$$

The proof is completed. □

Next, the ergodic capacity of U_1 is given as

$$\begin{aligned}
\bar{C}_1 =& \mathbb{E}\{\log_2(1+\bar{\gamma}_{U_1,\bar{x}_1})\} \\
=& \frac{1}{\ln 2}\int_0^\infty \frac{1}{x+1}\left[1-F_{\bar{\gamma}_{U_1,\bar{x}_1}}(x)\right]dx \\
=& \frac{1}{\ln 2}\int_0^{\frac{\hat{\xi}}{\hat{\zeta}}} \frac{1}{x+1}\left[1-F_{\gamma_1}\left(\frac{x}{\hat{\xi}-\hat{\zeta}x}\right)\right]dx \\
\overset{t=\frac{x}{\hat{\xi}-\hat{\zeta}x}}{=}& \frac{1}{\ln 2}\int_0^\infty \left(\frac{1}{t+(\hat{\xi}+\hat{\zeta})^{-1}} - \frac{1}{t+\hat{\zeta}^{-1}}\right)[1-F_{\gamma_1}(t)]dt,
\end{aligned} \tag{34}$$

where $\hat{\xi} = \rho d_1^{-\alpha}\varpi_1$ and $\hat{\zeta} = \rho d_1^{-\alpha}\left[\kappa_{D_2}^2\varpi_2 + \kappa_{D_1}^2\varpi_1\right]$.

From (34), $F_{\gamma_1}(t)$ is calculated by

$$\begin{aligned}
F_{\gamma_1}(u) =& 1 - \mathbb{P}_{LoS}(\theta_1)\Pr(\gamma_1 \geq u) - \mathbb{P}_{NLoS}(\theta_1)\Pr\left(\gamma_1 \geq \frac{u}{\omega}\right) \\
=& 1 - \mathbb{P}_{LoS}(\theta_1)e^{-K_1-\phi_1 t}\sum_{k=0}^{\infty}\sum_{q=0}^{\infty}\frac{K_1^{k+q}\phi_1^q t^q}{q!\Gamma(k+q+1)} \\
&- \mathbb{P}_{NLoS}(\theta_1)e^{-K_1-\omega^{-1}\phi_1 t}\sum_{k=0}^{\infty}\sum_{q=0}^{\infty}\frac{K_1^{k+q}\phi_1^q t^q}{q!\omega^q\Gamma(k+q+1)}.
\end{aligned} \tag{35}$$

Submitting (35) into (34) and solving for $\bar{\mathcal{C}}_2$, the close-form ergodic capacity at U_1 is attained as

$$\begin{aligned}\bar{\mathcal{C}}_1 =&\mathbb{P}_{LoS}(\theta_1)\sum_{k=0}^{\infty}\sum_{q=0}^{\infty}\frac{K_1^{k+q}\phi_1^q e^{-K_1}}{q!\Gamma(k+q+1)\ln 2}\left[\frac{1}{(\hat{\xi}+\hat{\zeta})^q}G_{1,2}^{2,1}\left(\frac{\phi_1}{\hat{\xi}+\hat{\zeta}}\middle|\begin{array}{c}1-q-1\\1-q-1,0\end{array}\right)\right.\\&\left.-\frac{1}{\hat{\zeta}^q}G_{1,2}^{2,1}\left(\frac{\phi_2}{\hat{\zeta}}\middle|\begin{array}{c}1-q-1\\1-q-1,0\end{array}\right)\right]+\mathbb{P}_{NLoS}(\theta_1)\sum_{k=0}^{\infty}\sum_{q=0}^{\infty}\frac{K_1^{k+q}\phi_1^q e^{-K_1}}{q!\Gamma(k+q+1)\ln 2}\\&\times\left[\frac{1}{\omega^q(\hat{\xi}+\hat{\zeta})^q}G_{1,2}^{2,1}\left(\frac{\phi_1}{\omega(\hat{\xi}+\hat{\zeta})}\middle|\begin{array}{c}1-q-1\\1-q-1,0\end{array}\right)-\frac{1}{\omega^q\hat{\zeta}^q}G_{1,2}^{2,1}\left(\frac{\phi_2}{\omega\hat{\zeta}}\middle|\begin{array}{c}1-q-1\\1-q-1,0\end{array}\right)\right].\end{aligned} \tag{36}$$

The ergodic capacity at U_1 is a function dependent on power coefficients, i.e., ϖ_1, ϖ_2, the LoS and NLoS propagation conditions, i.e., $\mathbb{P}_{LoS}$ and $\mathbb{P}_{NLoS}$, and the hardware impairment levels at the users, i.e., κ_{U_1} and κ_{U_2}, $\omega = 1$ represents LoS propagation and $\omega < 1$ represents NLoS propagation.

5. Numerical Results

In this part, we assign $\kappa = \kappa_{U_1}^2 = \kappa_{U_1}^2$, $K = K_1 = K_2$ and apply mathematical derivations to model the outage probability, which we then check with a Monte-Carlo simulation. The parameters utilized are listed in Table 1. Furthermore, the Monte-Carlo simulation is conducted 10^6 times to compare with the analytical results presented in the preceding section.

Table 1. Parameters.

Monte Carlo Simulations Repeated	10^6 Iterations
Target rates	$R_1 = 1.5$ & $R_2 = 1$
Power splitting factors	$\varpi_2 = 0.9$ & $\varpi_1 = 0.1$
The hardware impairments level	$\kappa = \kappa_{U_1}^2 = \kappa_{U_1}^2 = 0.01$
Path-loss factor	$\alpha = 2$
The UAV's altitude	$h = 1$
The radius round the trajectory	$r = 0.1$
The location of the ground users	$L = 1$
The UAV's location circle angle	$\varphi = 0$
Environment parameters	$p = 4.886$ & $q = 0.429$

Figure 2 illustrates the effect of the Rician-K factor K on the system performance and user outage probabilities. The simulation results are matched by the generated analytical and asymptotic equations. At large values of average SNR, we can see that the analytical results are in good agreement with the simulation results and the asymptotic curves work quite well at high SNR regimes, which corroborates the accuracy of our derivation. The outage probabilities of both users tend to decrease linearly when the SNR increases. The figure shows that the performance of U_2 is better than that of U_1. In addition, the outage probability increases as the value of K decreases. With the same K value, the outage probability of U_1 is always higher than that of U_2.

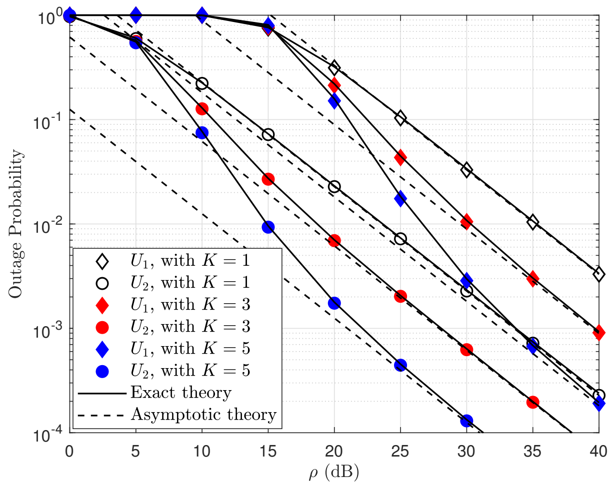

Figure 2. Outage probabilities of the users with different K values.

Figure 3 illustrates the outage probabilities of the two users versus SNR with $K = 2$, $R_1 = 1$ and $R_2 = 0.5$ under the effects of hardware impairment levels. It is observed that the higher the κ is, the higher is the outage probability. Moreover, U_2 always has a lower outage probability than U_1 regardless of the change of SNR and κ. In addition, the figure also shows that the outage probability of both users for the NOMA scheme is better than that for the OMA scheme.

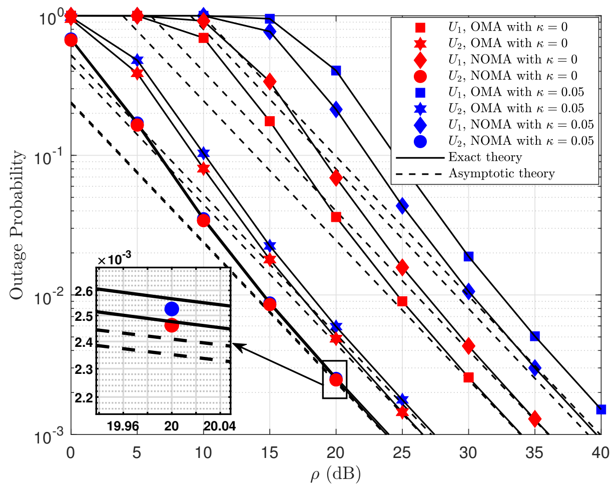

Figure 3. Outage probabilities of the users with $K = 3$, $R_1 = 1$ and $R_2 = 0.5$.

Figure 4 plots the outage probability of two users versus ϖ_2 in cases of $\kappa = 0.01$ and $\rho = 30$ (dB). The figure shows that the outage probabilities of the two users change according to the variation of ϖ_2. Specifically, the outage probability curves of U_1 first decrease in the ϖ_2 range from 0.5 to 0.6, then increase linearly in the ϖ_2 range from 0.6 to 0.9 and increase quickly in the ϖ_2 range from 0.9 to 1. The curves of the outage probability of U_2 decrease gradually in the overall range of ϖ_2. When K increases, the outage probabilities for both users always decrease. With the same K value, U_1 has a higher outage probability than U_2.

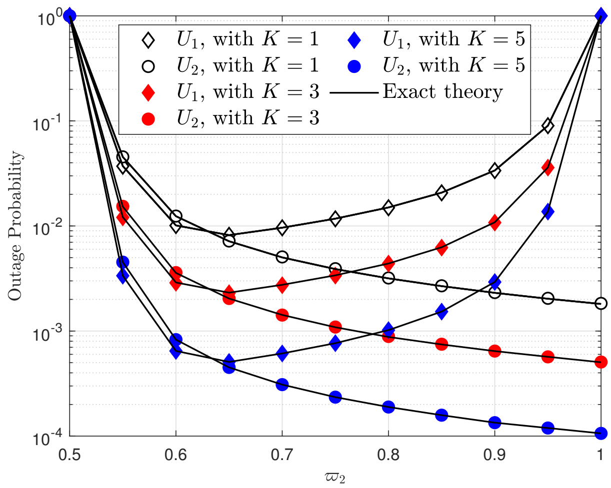

Figure 4. Outage probabilities of the users versus the power coefficient with $\kappa = 0.01$ and $\rho = 30$ (dB).

Figure 5 plots the outage probabilities of the two users versus φ with different r and K values. One can see from the figure that the outage probabilities of both U_1 and U_2 are almost constant for $r = 0.1, K = 1$, regardless of the change in φ. However, with $r = 0.9, K = 3$, the performances of the users have small changes. While the outage probability of U_1 decreases, that of U_2 increases in the φ range of -50 to 50 degrees. Especially, the outage probabilities of the two users reach maximum and minimum values at $\varphi = 0$ degrees.

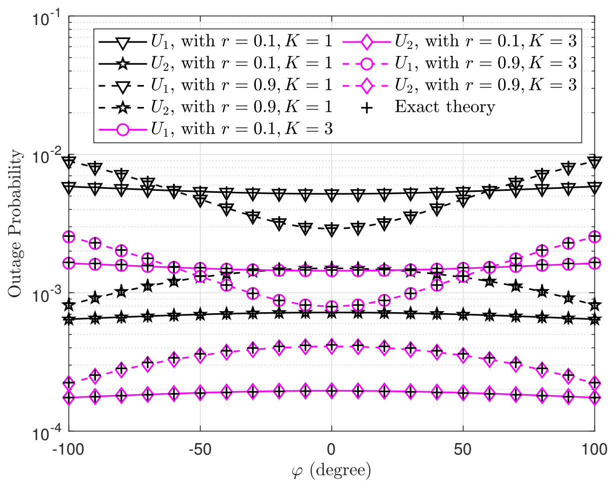

Figure 5. Outage probabilities of the users versus φ, with $R_1 = R_2 = 1$, $\kappa = 0.01$ and $\rho = 35$ (dB).

Figure 6 plots the ergodic capacity versus SNR in the case of $K = 5$ and $\omega = 0.1$. One can see that the ergodic capacity of U_1 is higher than that of U_2 in the case of $\kappa = 0$, i.e., with perfect hardware. However, when κ increases, herein $\kappa = 0.1$ and $\kappa = 0.2$, the ergodic capacity of U_2 is higher than that of U_1. This can be explained by understanding that when a hardware impairment level exists, only U_1 suffers the impacts of SNR. Besides, the higher the κ is, the lower the ergodic capacity is. Especially, the ergodic capacity for both users tends to be constant in the SNR range of 30 to 40 dB.

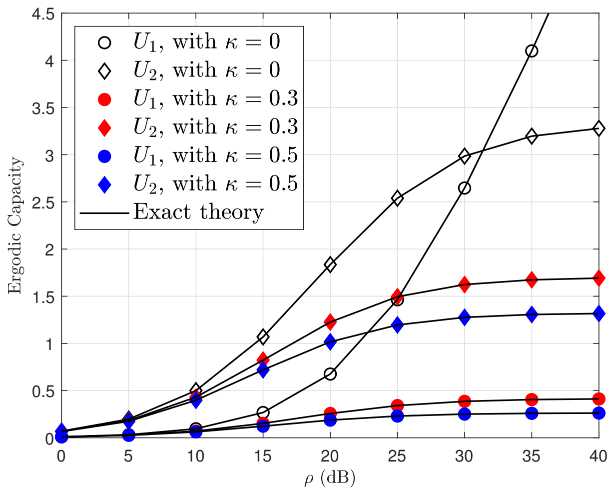

Figure 6. Ergodic capacity versus transmit SNR with $K = 5$ and $\omega = 0.1$.

In Figure 7, we investigate the ergodic capacity of UAVs at various heights with a transmit SNR of 40 dB. The lines of U_1 and U_2 are overlapped with each other for the optimal target rate, as shown in this diagram. As shown in Figure 7, the ergodic capacity decreases as the height of the UAV grows, implying that when the distance between the UAV and ground user is too great, the UAV will be unable to communicate with the ground users with the supplied transmit power. This is because the level of hardware degradation grows as the distance between the UAV and the users increases, resulting in a decrease in the users' ergodic capacity.

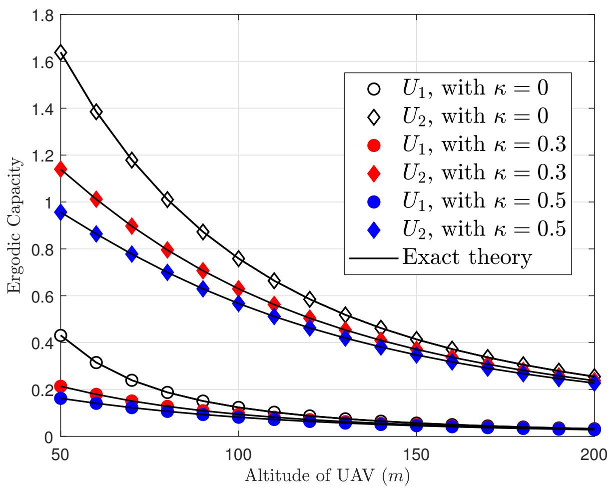

Figure 7. The ergodic capacity of U_1 and U_2 versus the altitude H of the UAV, with $K = 10$, $r = 0.9$, $\omega = 0.9$ and $\rho = 40$ (dB).

Finally, Figure 8 plots the ergodic capacity versus κ in the case of $\varpi_2 = 0.8$ or 0.9. One can observe that the ergodic capacity of both users decreases gradually when the value of κ increases from 0.1 to 1. This shows that the hardware impairment level seriously affects the performance of the system. Additionally, the ergodic capacity also changes when ϖ_2 varies from 0.7 to 0.9. Specifically, the higher the ϖ_2, the higher the ergodic capacity at U_2.

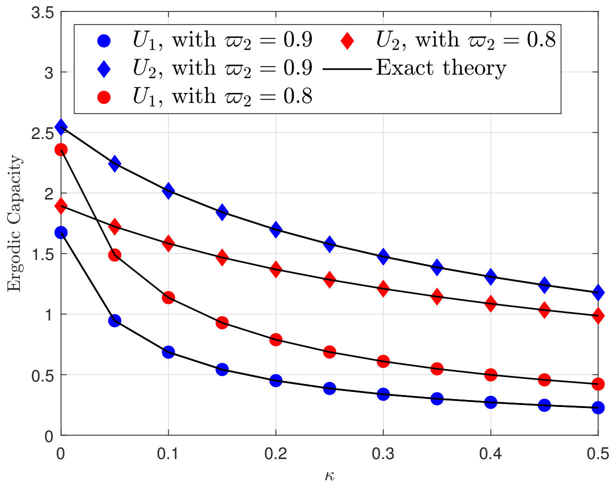

Figure 8. The ergodic capacities versus κ, with $K = 2$, $\omega = 0.5$, $r = 0.1$ and $\rho = 20$ (dB).

6. Conclusions

In this paper, we evaluated a UAV-enabled system deploying NOMA under hardware impairment. The exact and asymptotic expressions of the outage probability of the NOMA users and the ergodic capacity were derived. The results showed that the hardware impairment significantly affects the performance of the users in terms of the outage probabilities and the egodic capacities of the users. Moreover, depending on the hardware impairment level, only U_1 suffers from transmit SNR. In particular, in the case of perfect hardware, the ergodic capacity of U_1 is higher than that of U_2; however, there is an inverse phenomenon, i.e., the ergodic capacity of U_2 is higher than that of U_1, in imperfect hardware at a high SNR.

Author Contributions: Conceptualization, C.H.D., S.Q.N., C.-B.L. and N.T.V.K.; methodology, C.H.D. and S.Q.N.; formal analysis, C.-B.L. and N.T.V.K.; writing—original draft preparation, C.H.D.; writing—review and editing, S.Q.N.; funding acquisition, N.T.V.K. All authors have read and agreed to the published version of the manuscript.

Funding: The work of N.T.V. Khanh was supported by the University of Economics Ho Chi Minh City, Vietnam.

Conflicts of Interest: The authors declare no conflict of interest.

References

1. Small Unmanned Aerial Vehicles for Aerial Imaging, Recreation and Aerial Games. Global Market Analysis and Forecast. Available online: https://www.prnewswire.com/news-releases/consumer-drones--small-unmanned-aerial-vehicles-for-aerial-imaging-recreation-and-aerial-games-global-market-analysis-and-forecasts-300291554.html (accessed on 19 October 2021).
2. Liu, Y.; Dai, H.N.; Wang, Q.; Shukla, M.K.; Imran, M. Unmanned aerial vehicle for internet of everything: Opportunities and challenges. *Comput. Commun.* **2020**, *155*, 66–83. [CrossRef]
3. Filippone, A. *Flight Performance of Fixed and Rotary Wing Aircraft*; American Institute of Aeronautics & Ast (AIAA): Reston, VA, USA, 2006.
4. Shen, Y.; Pan, Z.; Liu, N.; You, X. Joint Design and Performance Analysis of a Full-Duplex UAV Legitimate Surveillance System. *Electronics* **2020**, *9*, 407. [CrossRef]
5. Wei, M.; Chen, Y.; Ding, M. On the Performance of UAV-Aided Content Caching in Small-Cell Networks with Joint Transmission. *Electronics* **2021**, *10*, 1040. [CrossRef]
6. Nguyen, P.X.; Nguyen, V.D.; Nguyen, H.V.; Shin, O.S. UAV-Assisted Secure Communications in Terrestrial Cognitive Radio Networks: Joint Power Control and 3D Trajectory Optimization. *IEEE Trans. Veh. Technol.* **2021**, *70*, 3298–3313. [CrossRef]
7. Nguyen, T.T.; Vu, T.H.; Nguyen, T.V.; Costa, D.B.d.; Ho, C.D. Underlay Cognitive NOMA-Based Coordinated Direct and Relay Transmission. *IEEE Wirel. Commun. Lett.* **2021**, *10*, 854–858. [CrossRef]
8. Nguyen, T.T.; Nguyen, T.V.; Vu, T.H.; Costa, D.B.d.; Ho, C.D. IoT-Based Coordinated Direct and Relay Transmission with Non-Orthogonal Multiple Access. *IEEE Wirel. Commun. Lett.* **2021**, *10*, 503–507. [CrossRef]
9. Sharma, P.K.; Kim, D.I. UAV-Enabled Downlink Wireless System with Non-Orthogonal Multiple Access. In Proceedings of the 2017 IEEE Globecom Workshops (GC Wkshps), Singapore, 4–8 December 2017; pp. 1–6. [CrossRef]

10. Wu, Q.; Xu, J.; Zhang, R. Capacity Characterization of UAV-Enabled Two-User Broadcast Channel. *IEEE J. Sel. Areas Commun.* **2018**, *36*, 1955–1971. [CrossRef]
11. Sohail, M.F.; Leow, C.Y.; Won, S. Non-Orthogonal Multiple Access for Unmanned Aerial Vehicle Assisted Communication. *IEEE Access* **2018**, *6*, 22716–22727. [CrossRef]
12. Liu, X.; Wang, J.; Zhao, N.; Chen, Y.; Zhang, S.; Ding, Z.; Yu, F.R. Placement and Power Allocation for NOMA-UAV Networks. *IEEE Wirel. Commun. Lett.* **2019**, *8*, 965–968. [CrossRef]
13. Tang, R.; Cheng, J.; Cao, Z. Joint Placement Design, Admission Control, and Power Allocation for NOMA-Based UAV Systems. *IEEE Wirel. Commun. Lett.* **2020**, *9*, 385–388. [CrossRef]
14. Mu, X.; Liu, Y.; Guo, L.; Lin, J. Non-Orthogonal Multiple Access for Air-to-Ground Communication. *IEEE Trans. Commun.* **2020**, *68*, 2934–2949. [CrossRef]
15. Pang, X.; Tang, J.; Zhao, N.; Zhang, X.; Qian, Y. Energy-efficient design for mmWave-enabled NOMA-UAV networks. *Sci. China Inf. Sci.* **2021**, *64*, 1–14. [CrossRef]
16. Zhao, N.; Pang, X.; Li, Z.; Chen, Y.; Li, F.; Ding, Z.; Alouini, M.S. Joint trajectory and precoding optimization for UAV-assisted NOMA networks. *IEEE Trans. Commun.* **2019**, *67*, 3723–3735. [CrossRef]
17. Tung, N.T.; Nam, P.M.; Tin, P.T. Performance evaluation of a two-way relay network with energy harvesting and hardware noises. *Digit. Commun. Netw.* **2021**, *7*, 45–54. [CrossRef]
18. Zhu, J.; Ng, D.W.K.; Wang, N.; Schober, R.; Bhargava, V.K. Analysis and Design of Secure Massive MIMO Systems in the Presence of Hardware Impairments. *IEEE Trans. Wirel. Commun.* **2017**, *16*, 2001–2016. [CrossRef]
19. Guo, K.; An, K.; Zhang, B.; Huang, Y.; Zheng, G. Outage Analysis of Cognitive Hybrid Satellite-Terrestrial Networks with Hardware Impairments and Multi-Primary Users. *IEEE Wirel. Commun. Lett.* **2018**, *7*, 816–819. [CrossRef]
20. Li, X.; Li, J.; Liu, Y.; Ding, Z.; Nallanathan, A. Residual Transceiver Hardware Impairments on Cooperative NOMA Networks. *IEEE Trans. Wirel. Commun.* **2020**, *19*, 680–695. [CrossRef]
21. Deng, C.; Liu, M.; Li, X.; Liu, Y. Hardware Impairments Aware Full-Duplex NOMA Networks over Rician Fading Channels. *IEEE Syst. J.* **2021**, *15*, 2515–2518. [CrossRef]
22. Masaracchia, A.; Nguyen, L.D.; Duong, T.Q.; Yin, C.; Dobre, O.A.; Garcia-Palacios, E. Energy-efficient and throughput fair resource allocation for ts-noma uav-assisted communications. *IEEE Trans. Commun.* **2020**, *68*, 7156–7169. [CrossRef]
23. Li, X.; Wang, Q.; Liu, Y.; Tsiftsis, T.A.; Ding, Z.; Nallanathan, A. UAV-aided multi-way NOMA networks with residual hardware impairments. *IEEE Wirel. Commun. Lett.* **2020**, *9*, 1538–1542. [CrossRef]
24. Tang, X.; An, K.; Guo, K.; Huang, Y. Outage analysis of non-orthogonal multiple access-based integrated satellite-terrestrial relay networks with hardware impairments. *IEEE Access* **2019**, *7*, 141258–141267. [CrossRef]
25. Ono, F.; Ochiai, H.; Miura, R. A wireless relay network based on unmanned aircraft system with rate optimization. *IEEE Trans. Wirel. Commun.* **2016**, *15*, 7699–7708. [CrossRef]
26. Simon, M.K.; Alouini, M.S. *Digital Communication over Fading Channels*; John Wiley & Sons: Hoboken, NJ, USA, 2005; Volume 95.
27. Gradshteyn, I.S.; Ryzhik, I.M. *Table of Integrals, Series and Products*; Academic Press: Cambridge, MA, USA, 2014.
28. Mozaffari, M.; Saad, W.; Bennis, M.; Debbah, M. Unmanned aerial vehicle with underlaid device-to-device communications: Performance and tradeoffs. *IEEE Trans. Wirel. Commun.* **2016**, *15*, 3949–3963. [CrossRef]
29. Yang, S.; Deng, Y.; Tang, X.; Ding, Y.; Zhou, J. Energy efficiency optimization for UAV-assisted backscatter communications. *IEEE Commun. Lett.* **2019**, *23*, 2041–2045. [CrossRef]
30. Prudnikov, A.P.; Brychkov, Y.A.; Marichev, O.I. *Integrals and Series, Volume 3: More Special Functions*; Gordon and Breach: New York, NY, USA; London, UK, 1986; Volume 55.